Aerospace Science and Technology 147 (2024) 109033

Contents lists available at ScienceDirect

Aerospace Science and Technology

journal homepage: www.elsevier.com/locate/aescte

Design considerations for efficient spanwise-inclined air-jet vortex generators for separation control in supersonic and hypersonic flows

Robin Sebastian *, Anne-Marie Schreyer

RWTH Aachen University, 52062 Aachen, Germany

ARTICLE INFO

Communicated by Mehdi Ghoreyshi

Keywords:
Large eddy simulation
Air-jet vortex generator
Separation control
Jet in crossflow

ABSTRACT

Shock-wave/boundary-layer interactions and associated flow separation are frequently occurring phenomena in many high-speed flow applications. Injection of spanwise-inclined air-jets is an efficient means to control shock-induced flow separation in supersonic and transonic flows. Separation-control studies in hypersonic flow are scarce and so far mostly restricted to microramp control. The objectives of the current work are to broaden the scope into hypersonic regime, investigate the influence of crossflow Mach and Reynolds number on the jet-injection flow field, and to find a suitable control parameter that is valid across a wide range of flow conditions. For this purpose, we study injection of a single spanwise-inclined jet in supersonic and hypersonic crossflows using large-eddy simulations. We analyzed the flow topology, induced vortical structures and boundary-layer statistics. The general characteristics of the jet/crossflow interactions are similar in the supersonic and hyperonic regimes: the injection of a spanwise-inclined jet induces an asymmetric flow topology with a complex system of shocks and vortical structures. We identified the ratio of injection-pressure-to-freestream-pressure as a suitable parameter to characterize and compare jet/crossflow interactions in different flow regimes. In addition, we recommend larger boundary-layer-to-jet-diameter ratio for control applications, because it delays the lift-off of major vortices. The present results suggest that rows of spanwise-inclined jets can be efficiently used to control separation also in hypersonic flow. Moreover, low momentum-flux jet injection can be potentially also used for cooling purposes.

1. Introduction

Shock wave/boundary interactions (SWBLI) occur in flow fields within and around high-speed vehicles under a wide range of conditions. When the shock wave is too strong, it causes large-scale separation, resulting in flow distortion and a significant loss of total pressure. Moreover, the unsteadiness associated with SWBLI can cause high temperature and pressure loads on the structure of the vehicle. These effects make it important to investigate methods to avoid or mitigate shock-induced flow separation and/or modulate the frequency of the unsteadiness in order to tune it away from the structural resonance.

Various control techniques, such as boundary layer bleed/suction [1], mechanical vortex-generators (MVGs) [2], and air-jet vortex-generators (AJVGs) [3] have been developed in recent years to minimize the detrimental effects of SWBLI. While the bleed technique and MVGs are effective at suppressing flow separation, they also have an impact on the overall performance of the system. Boundary-layer bleed, for example, reduces the achievable overall thrust in engine applications [4]. MVGs induce additional drag and are only fully adapted to a specific set of flow conditions (see e.g. [5,6]). As a result, such systems lack operational flexibility. These disadvantages can be overcome by using AJVGs, where small air jets are injected into the crossflow to induce streamwise vortices with a comparable control effectiveness as those generated by MVGs [7]. AJVGs offer greater flexibility than mechanical devices: they can be turned off when not needed (thus reducing the induced parasitic drag), and they can also be combined with cooling [8].

The effectiveness of an AJVG setup is determined by a number of geometric and flow parameters. Several studies revealed the effects of geometric parameters (such as jet orientation, jet diameter, jet spacing, and their arrangement) and flow parameters (such as jet injection pressure, velocity, density, momentum flux, and temperature) on control efficiency (see e.g. [9–12]). Wallis [13] found that injecting spanwise-inclined jets is more effective for controlling flow separation than wall-normal or streamwise injection.

* Corresponding author.
E-mail address: r.sebastian@aia.rwth-aachen.de (R. Sebastian).

https://doi.org/10.1016/j.ast.2024.109033
Received 27 October 2023; Received in revised form 22 February 2024; Accepted 29 February 2024
Available online 5 March 2024

Table 1
Global flow parameters.

Crossflow	M_∞	$\tilde{T}_0$/K	$\tilde{p}_0$/Pa	$\tilde{u}_\infty$/ms^{-1}	Re_θ	$\tilde{\delta}_{99} \times 10^3$/m	Re_τ
C1	7.2	760	7930000	1180	3500	4.3	215
C2	2.5	295	101325	578	1570	2.0	245
C3	2.5	295	101325	578	7000	9.4	1093

Table 2
Details of the parameters and cases studied.

No.	Variable	Cases		Constant conditions
1	p^{pl}/p_∞	M7.2a $p^{pl}/p_\infty = 10$	M7.2b $p^{pl}/p_\infty = 15$	$Re_\tau = 215$, $M_\infty = 7.2$, $\delta_{99}/d \approx 5$
2	δ_{99}/d	M7.2b $\delta_{99}/d \approx 5$	M7.2c $\delta_{99}/d \approx 10$	$Re_\tau = 215$, $M_\infty = 7.2$, $p^{pl}/p_\infty = 15$
3	M_∞	M7.2c $M_\infty = 7.2$	M2.5a $M_\infty = 2.5$	$Re_\tau \approx 215 - 245$, $p^{pl}/p_\infty = 15 - 17$, $\delta_{99}/d \approx 10$
4	Re_τ	M2.5a $Re_\tau = 245$	M2.5b $Re_\tau = 1093$	$p^{pl}/p_\infty = 17$, $\delta_{99}/d \approx 10$, $M_\infty = 2.5$

Due to the complexity of the flow, a majority of these studies are experimental, and the resolution of details in the near field of jet injection is challenging. Detailed information on the jet flow and near-field flow organization past injection was missing until recently. The development of high performance computation (HPC), now enables high-fidelity simulations of such complex flow problems. We recently performed a large-eddy simulation (LES) of the injection of a spanwise-inclined jet in a supersonic crossflow (JISCF) on a flat plate at $M_\infty = 2.5$ and $Re_\theta = 7000$ [14], and analyzed the jet flow, the dynamic behavior of the jet/crossflow interaction, as well as the flow past injection.

To develop efficient and flexible AJVG control for aerospace applications, we need a better understanding of the physics and governing mechanisms in the flow field around spanwise-inclined jets across a wide range of Mach numbers. Spanwise-inclined AJVGs are an effective separation control technique in the transonic and supersonic flow regimes (see e.g. [3,10,15]). Separation-control studies in hypersonic flow are particularly scarce and so far mostly restricted to microramp control (see e.g. [16,17]). The primary objective of the current work is to broaden the scope and understanding of AJVG control into the hypersonic regime. This requires investigating the influence of crossflow Mach and Reynolds number on the jet-injection flow field. Moreover, varying conditions in the supersonic and hypersonic flow regimes make it important to understand the effects of other parameters on the jet-crossflow interactions in the different flow regimes. Hence, the present study also investigates the effect of parameters, such as the injection pressure and boundary-layer-to-jet-diameter, to find a suitable control parameter that is valid across a wide range of flow conditions.

In the present work, we therefore perform LESs of a single spanwise-inclined jet injected into a hypersonic crossflow (JIHCF) at $M_\infty = 7.2$, $Re_\theta = 3500$ and JISCF at $M_\infty = 2.5$, $Re_\theta = 1570$ (see Table 1 for the flow parameters). These hypersonic flow conditions are similar to the experimental conditions reported in Schreyer et al. [18] and supersonic conditions are similar to the direct numerical simulation (DNS) of Guarini et al. [19] to allow for comparisons. An adiabatic wall is considered in the supersonic case, whereas the hypersonic case has a cold wall with $T_w = 340$ K ($T_w/T_r \approx 0.5$; T_r is the adiabatic wall temperature); these conditions match the reference DNS by Priebe et al. [20] and the experiment by Schreyer et al. [18]. The characteristics of the injected jet, as well as the jet/crossflow interaction in the injection near-field and their dynamics are mainly affected by the injection geometry [21] and pressure [22], and additionally by the jet-spacing in the case of an array of jets [23]. The influence of wall temperature on the near-field characteristics is small. Influences of the different wall-temperature conditions on the evolution of the flow in the mid- and far-field of injection are not considered here, and are outside the scope of the objectives of the present work.

To understand the influence of crossflow Mach and Reynolds number on the jet/crossflow interaction and to find out if there is a suitable set of control parameters that is valid across a wide range of flow conditions, we studied three JIHCF cases (M7.2a, M7.2b and M7.2c in Table 3) and two JISCF cases M2.5a and M2.5b. Case M2.5b was taken from our previous work [14]. In the present work, we investigate the effects of injection-pressure-to-freestream-pressure, p^{pl}/p_∞ (using cases M7.2a and M7.2b), boundary-layer-to-jet-diameter, δ_{99}/d (using cases M7.2b and M7.2c), cross-flow Mach number M_∞ (using cases M7.2c and M2.5a), and friction Reynolds number Re_τ (using cases M2.5a and M2.5b). Variables p^{pl}/p_∞, M_∞ and Re_τ are flow parameters, whereas, δ_{99}/d is a hybrid parameter involving a flow parameter (δ_{99}) and a geometric parameter (d). The value of δ_{99}/d can be fixed either by changing the position of the jet in the developing boundary layer or the jet diameter. We change the diameter of the jet (in case M7.2c) to fix a value for δ_{99}/d. We can therefore maintain the same characteristics for the crossflow boundary layer into which the jet is injected. To investigate the effects of Re_τ, one has to consider crossflows with different characteristics. Therefore, in order to maintain a constant δ_{99}/d we varied d in accordance with δ_{99} of the crossflow. The test cases are listed in Table 2. Our approach involved four steps: first, the jet-injection pressure (which is a flow parameter) was varied in cases M7.2a and M7.2b, while maintaining all other parameters constant. This allows us to (a) study the influence of injection pressure in a JIHCF, and (b) compare the influence of injection pressure on jet injection in supersonic and hypersonic crossflows. In our recent study [22], we showed that the injection pressure affects the formation of the secondary upper-trailing vortex in a supersonic crossflow, which is crucial in introducing the asymmetry of the major counter-rotating vortex pair (CVP). The size and strength of the major CVP, and the associated flow asymmetry strengthen with the injection pressure $p^{pl}/p_\infty \geq 15$ [22].

Then, in case M7.2c, the injection-pipe diameter (which is a geometric parameter) was decreased to investigate the influence of δ_{99}/d on the jet/crossflow interactions.

Next, in case M2.5a, the crossflow Mach number was reduced to match case M2.5b, while maintaining all other parameters as in case M7.2c. This approach also allows to analyze the influence of crossflow (a) Mach number by comparing cases M7.2c and M2.5a, (b) Reynolds number (Re) by analyzing cases M2.5a and M2.5b. Details of all parameters in this systematic parametric study are given in Table 2.

The numerical methods and computational setup used in this work are discussed in Sec. 2 and 3, respectively. The results are presented in

Sec. 4, and finally, the findings and concluding remarks are summarized in Sec. 5.

2. Numerical methods

LESs were performed using the finite-volume solver m-AIA (formerly known as ZFS) [24] on a body-fitted block-structured mesh, using the monotonically integrated LES (MILES) approach to provide an efficient implicit LES framework [25]. The convective fluxes are discretized using a second-order accurate advection upstream splitting method (AUSM) [26], and the viscous fluxes are discretized with a modified cell-vertex scheme at second-order accuracy [27]. The monotone upstream scheme for conservation laws (MUSCL) with the Venkatakrishnan limiter [28] is used to reconstruct the cell surface values and prevent steep and strong shocks from creating non-physical oscillations. The time integration is performed with a second-order accurate 5-stage Runge-Kutta scheme. The effects of the subgrid-scale model and order of the method on the overall accuracy of the solution have been discussed by Meinke et al. [27]. The numerical method has been thoroughly validated and proven suitable for the present case by computing flow problems such as turbulent boundary layers [29], shock-wave/boundary-layer interactions [30,31], and jets of different configurations in supersonic crossflow [22,23,32,33], as well as separation control with air-jet vortex generators [34].

Unless specified otherwise, the following non-dimensionalization is used for the velocity $\mathbf{u} = \tilde{\mathbf{u}}/\tilde{a}_0$, where the speed of sound is $\tilde{a}_0 = \sqrt{\gamma \tilde{p}_0/\tilde{\rho}_0}$; $\tilde{\cdot}$ denotes dimensional quantities, and subscript "0" denotes values at stagnation condition. The temperature, density, and pressure are non-dimensionalized as $T = \tilde{T}/\tilde{T}_0$, $\rho = \tilde{\rho}/\tilde{\rho}_0$, and $p = \tilde{p}/\tilde{\rho}_0\tilde{a}_0^2$, respectively, and the viscosity is expressed using Keyes's law [20] in the hypersonic case and Sutherland's law in the supersonic case. The lengths and distances are non-dimensionalized using the injection-pipe diameter d, such that $\mathbf{x} = \tilde{\mathbf{x}}/\tilde{d}$. Time-averaged quantities and fluctuations are denoted with $<\cdot>$ and the superscript $'$, respectively. Time- and spanwise- averaged quantities are denoted with $\overline{\cdot}$. Furthermore, we use the following subscripts: "∞", "δ_{99}", and "w" for values in the freestream, at the edge of the boundary layer, and at the flat-plate surface (wall), respectively; "θ", "τ", "d" for quantities based on the momentum thickness, wall shear stress, and injection-pipe diameter, respectively; and "x", "y", "z" for streamwise, wall-normal, and spanwise quantities, respectively. The following superscripts are used: "+" for values scaled in viscous units; "vd" for van Driest scaled quantities; "jet" for values at the jet exit; and "cf","pl" for quantities related to the crossflow and plenum subdomains, respectively.

3. Computational setup and conditions

The geometry of a single spanwise-inclined jet injected into a boundary layer on a flat plate that we study here is shown in Fig. 1(a). The computational domain consists of (a) a plenum below the flat-plate surface (which supplies the air needed for injection), (b) a pipe (which is used to inject the jet), and (c) a flat plate (where the jet is injected into the oncoming crossflow). A fully developed turbulent boundary layer on the flat-plate surface served as the cross flow, see Table 1 for more details on the different crossflows considered.

The origin $\mathbf{O}(0,0,0)$ of the coordinate system is at the jet-injection location on the flat-plate surface. A sufficiently long distance ($l1 = 37\delta_{99}$ for cases M7.2a, M7.2b and M7.2c, and $l1 = 23\delta_{99}$ for case M2.5a and M2.5b) between the inlet of the cross-flow subdomain and the jet-injection location ensures the transition of the cross flow to a fully developed turbulent state. Downstream of the injection location, the cross-flow domain extends up to $l2 = 100d$, allowing to study the flow physics in both the near- and far-field downstream of the jet injection, which is of particular interest for flow control applications. The streamwise, wall-normal and spanwise extents of the cross-flow subdomain are $L_x^{\mathrm{cf}} = l1 + l2$, $L_y^{\mathrm{cf}} = 6.5\delta_{99}$, and $L_z^{\mathrm{cf}} = 32d$, respectively. The plenum has the dimensions $L_x^{\mathrm{pl}} \times L_y^{\mathrm{pl}} \times L_z^{\mathrm{pl}} = 14d \times 13d \times 8d$, and it is located at a distance $s = 3d$ beneath the surface of the flat plate.

In the JISCF cases, the boundary layer-to-pipe diameter ratio is $\delta_{99}/d \approx 10$, whereas, for the JIHCF cases we considered two values of $\delta_{99}/d \approx 5$ and 10, respectively. The reason for this variation in δ_{99}/d is to examine the influence of injection pipe diameter on the induced vortical structures and the jet-injection flow field, particularly on the jet penetration depth and lift off of major CVP. The pipe is spanwise-inclined at an angle of $\alpha = 45°$ (in the $y-z$ plane), and has a yaw angle of $\beta = 270°$ (in the $x-z$ plane) with respect to the $x-$axis. Due to the spanwise inclination, both ends of the pipe have an elliptical cross section: the major axis of the pipe exit cross section on the flat-plate surface aligns with the $z-$axis and the minor axis aligns with the $x-$axis.

To accurately capture the influence of a spanwise-inclined JISCF and JIHCF problem, a DNS-like resolution is used near the flat plate. The mesh is gradually relaxed in the wall-normal direction. The mesh resolution in the crossflow region guarantees $\Delta x^+ \leq 10$, $\Delta y_w^+ = 1$, $\Delta y_{\delta_{99}}^+ = 12$, and $\Delta z^+ \leq 5$ in the supersonic cases and $\Delta x^+ \leq 10$, $\Delta y_w^+ = 0.5$, $\Delta y_{\delta_{99}}^+ = 5$, and $\Delta z^+ \leq 5$ in the hypersonic cases. In the supersonic cases, these mesh resolutions were chosen based on a grid-sensitivity study for boundary layer case C3 with $Re_\tau = 1093$ reported in Refs. [14,21]. The grid resolution used in the supersonic case C3 was found suitable with an uncertainty of 1.1% on the u_τ estimation with respect to the comparable experimental study at similar conditions [14,15,23]. As a result, both the inner- and outer-layer of the boundary-layer flow are accurately captured (see Fig. 3 in [33]). The grid resolution used in case C3 also discretizes the C2 boundary layer accurately, which does not require additional mesh refinement due to its lower $Re_\tau = 245$. In the hypersonic case, the aforementioned mesh resolutions match the DNS study of Priebe et al. [20], and the estimated skin friction coefficient c_f is in good agreement with both the experiment by Schreyer et al. [18] and the DNS [20] at similar conditions (present case: 0.00107, Exp.: 0.00095 and DNS: 0.0011). Refining the grid for an implicit LES makes the simulation equivalent to a DNS [14], and currently the error on c_f is only 2.8%. Moreover, the turbulent structures are more coherent due to the altered energy transfer mechanism with the cold wall. These structures are approximately 30% larger in the cold wall case (with $T_w/T_r \approx 0.5$) than with the adiabatic wall [35]. For an unchanged mesh size, the structures would thus already be discretized by a larger number of cells. We did, however, approximately half the mesh spacing in the wall-normal direction compared to the adiabatic case. With this finer grid, the uncertainty is thus minimized, and, therefore, an additional mesh dependence study is not required to validate the present hypersonic case.

About 125 points in the wall-normal direction are used to discretize the low Re_τ crossflow boundary layers. Due to the very similar jet injection configurations in the hypersonic and supersonic cases, we generated a block-structured mesh resembling the characteristics of the mesh used in the supersonic case in our previous study [14] for the hypersonic case as well. The computational mesh in the vicinity of the jet orifice is shown in Fig. 1(b). In the vicinity of the jet-injection location, a finer grid resolution is used in all directions. In the radial direction, the first mesh point from the pipe surface is located at $\Delta r_w^+ = 0.5$. A mesh resolution similar to the crossflow subdomain was used to discretize the plenum in the x and z directions. In the y direction, the first point from the top surface of the plenum is located at $\Delta y^+ = 0.5$, and the mesh is gradually coarsened in the $-y$ direction. Mesh points were clustered at both ends of the pipe to (a) ensure a smooth transition between different regions of the computational domain (plenum/pipe and pipe/crossflow) and (b) accurately capture the flow physics with great detail (see Fig. 1(b)).

Synthetic turbulence was injected into the crossflow through the inflow plane [36]. In the hypersonic cases, an isothermal no-slip wall boundary condition was used at the flat-plate surface with $\tilde{T}_w = 340$ K, similar to the flow conditions of Schreyer et al. [18] and Priebe et al. [20]. Whereas, in the supersonic cases, the adiabatic no-slip wall con-

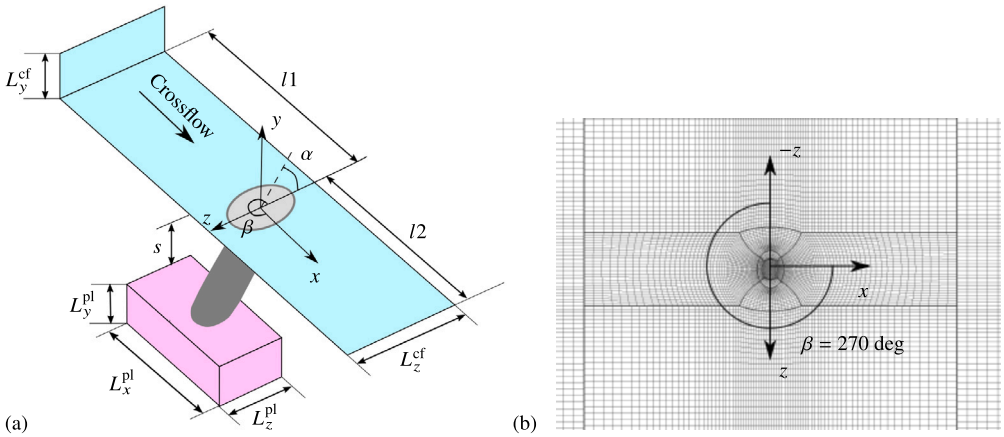

Fig. 1. (a) Schematic representation of the flow configuration (not to scale). (b) Zoom of the cross-flow subdomain in the vicinity of the jet-injection location (wall-parallel plane at $y = 0$) showing every 5th node.

ditions were used. In all cases, the adiabatic wall boundary condition was used at the pipe surface, top, and side faces of the plenum. We imposed an outflow boundary condition on the top surface and the outflow plane of the crossflow region, and used a periodic boundary condition in the spanwise direction of the crossflow subdomain. The crossflow was initialized with the mean flow field computed from a corresponding Reynolds Averaged Navier-Stokes (RANS) simulation, which was used by the synthetic turbulence generator to feed the crossflow with realistic turbulence. The pipe and plenum were initialized with a zero velocity field and the free-stream density and pressure. The jet was injected into the crossflow by prescribing the desired pressure at the bottom face of the plenum. The plenum injection pressure was linearly ramped up from freestream pressure to the desired value. In all cases, the temperature at the bottom face of the plenum was set equal to T_0.

Simulations were performed on the HPE APOLLO HPC facility at HLRS, Stuttgart, with approximately 0.7×10^6 core hrs, and the data are available on request.

3.1. Studied cases

To study the effect of different geometric and flow parameters on the jet/crossflow interaction, we performed simulations of single spanwise-inclined jets in a crossflow at $M_\infty = 7.2$ and $Re_\theta = 3500$ (cases M7.2a, M7.2b and M7.2c), $M_\infty = 2.5$ with $Re_\theta = 1570$ (case M2.5a) and 7000 (case M2.5b). To find a suitable control parameter which is valid across a wide range of flow regime, we first varied the injection pressure in the hypersonic cases M7.2a and M7.2b. The characteristics and dynamics of the injected jet are primarily affected by the difference between the injection and the freestream pressure. For the case of a single jet in supersonic crossflow, the influences of the injection pressure on the characteristics of the jet and the near-field jet/crossflow interactions have been discussed in [22]. In cases M7.2b and M7.2c, we varied the diameter of the injection pipe which is a geometric parameter to analyze the influence δ_{99}/d on the jet/crossflow interactions. In cases M7.2a and M7.2b we considered $\delta_{99}/d \approx 5$ ($\tilde{d} = 1$ mm). The injection pressure was increased from $p^{pl}/p_\infty = 10$ to 15 in case M7.2b, while maintaining all other parameters constant as in case M7.2a. The counter-clockwise rotating (CCR) upper-trailing secondary vortex is only formed at sufficiently high injection pressures [22], and it is responsible for the formation of asymmetric major CVP. Hence, comparison of the influence of injection pressure in JIHCF and JISCF will help to verify the suitability of injection pressure as a control parameter over a wide range of crossflow Mach numbers. In case M7.2c, the injection pipe diameter was reduced such that $\delta_{99}/d \approx 10$ ($\tilde{d} = 0.5$ mm), while keeping other parameters unchanged as in case M7.2b. Due to the difference in the characteristics of the supersonic and hypersonic boundary layers, the injection pipe diameter was varied such that we have an equivalent δ_{99}/d in cases M7.2c, M2.5a and M2.5b. This allows to analyze the influence of injection pipe diameter on the penetration depth, and on the major CVP, particularly its lift off and resulting influence on the downstream flow. Moreover, comparison of cases M7.2c and M2.5a also allows to study the effects of crossflow Mach number on the jet/crossflow interactions. Analysis of cases M2.5a and M2.5b gives more insight into the effects of crossflow friction Reynolds number on the jet/crossflow interactions. The results were compared with our earlier study of single spanwise-inclined JISCF at $M_\infty = 2.5$ and $Re_\theta = 7000$ with $\tilde{d} = 1$ mm and $p^{pl}/p_\infty = 17$ (case M2.5b) [14], to find optimal injection parameters which will serve to improve the flexibility of AJVG setups used for control application across a wide range of flow regimes.

In addition to the jet injection cases, we also performed a simulation of an undisturbed boundary layer on a flat plate at the same Mach and Reynolds numbers as the jet injection cases for validation purposes. For reference, the main flow parameters are given in Table 1, and the test cases are listed in Tables 2 and 3.

4. Results

In the following sections, we will first present the oncoming crossflows at $M_\infty = 7.2$, $Re_\theta = 3500$ and $M_\infty = 2.5$, $Re_\theta = 1570$ (Sec. 4.1), followed by a discussion on the flow in the jet-injection pipe in Sec. 4.2. The resulting jet/crossflow interaction is discussed by analyzing the general flow topology in Sec. 4.3, coherent vortical structures in Sec. 4.4, and boundary-layer statistics in Sec. 4.5.

4.1. Oncoming crossflow

The hypersonic crossflow represents a fully developed low Reynolds number turbulent boundary-layer flow with $Re_\theta = 3500$ and $Re_\tau = 215$, and the supersonic crossflow with $Re_\theta = 1570$ and $Re_\tau = 245$. The hypersonic boundary-layer profiles were validated against the experimental results of Schreyer et al. [18] (labeled as Sch.2018 in Fig. 2) and DNS data of Priebe et al. [20] (labeled as Prb.2011), and the supersonic boundary layer is compared with a reference DNS by Guarini et al. [19] (labeled as Gua.2000) at similar M_∞ and Re_θ. Both mean and RMS profiles have satisfactory agreement with the experimental and DNS data (see Fig. 2). The mean velocity collapses on the DNS data, with a slightly higher log-law constant due to the isothermal walls in the hypersonic case [20]. Similarly, the mean velocity profile of the hypersonic case agrees with the experimental data up to $y^+ = 200$. Compared to the experiment, the boundary-layer thickness in the hypersonic case is smaller in the simulations. Hence, the velocity in the wake region is underestimated. Due to the cold wall, the slope of the viscous sub-layer is reduced [37], and an early departure from the $y^+ = \overline{u}^+$ is observed in the hypersonic case. The Morkovin-scaled RMS of the streamwise and wallnormal

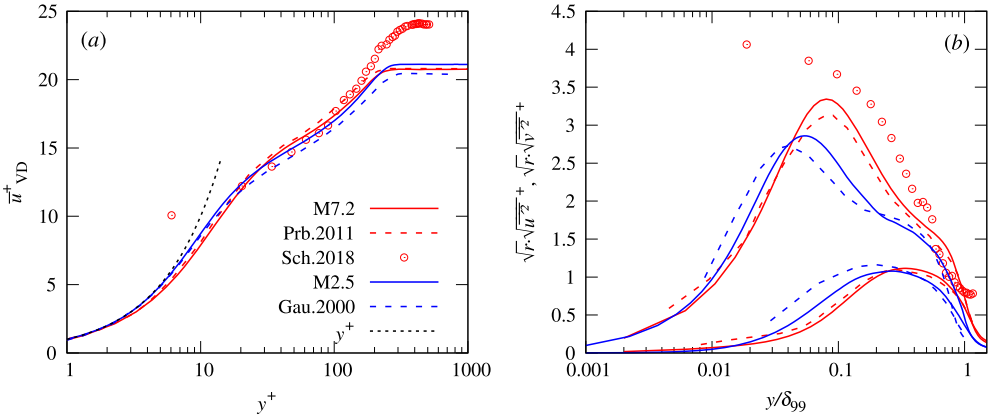

Fig. 2. Incoming boundary layer profiles for $M_\infty = 7.2$, $Re_\theta = 7000$ (red) and $M_\infty = 2.5$, $Re_\theta = 1570$ (blue). (a) vanDriest transformed mean velocity, and (b) Morkovin scaled profiles of the rms of velocity components. (For interpretation of the colors in the figure(s), the reader is referred to the web version of this article.)

Table 3
Simulation test cases and results.

Cases	M_∞	δ_{99}/d	p^{pl}/p_0	p^{pl}/p_∞	ρ^{pl}/ρ_0	ρ^{pl}/ρ_∞	p^{jet}/p_∞	V^{jet}/V_∞	ρ^{jet}/ρ_∞	J	C_μ
M7.2a	7.2	≈ 5	0.002	10	0.002	0.87	4.94	0.48	0.5	0.085	0.0010
M7.2b	7.2	≈ 5	0.003	15	0.003	1.31	7.46	0.54	0.67	0.13	0.0015
M7.2c	7.2	≈ 10	0.003	15	0.003	1.31	7.1	0.53	0.63	0.11	0.0006
M2.5a	2.5	≈ 10	1.0	17	1.0	7.6	8.93	0.89	2.86	1.39	0.0068
M2.5b	2.5	≈ 10	1.0	17	1.0	7.6	9.3	0.90	3.18	1.52	0.0080

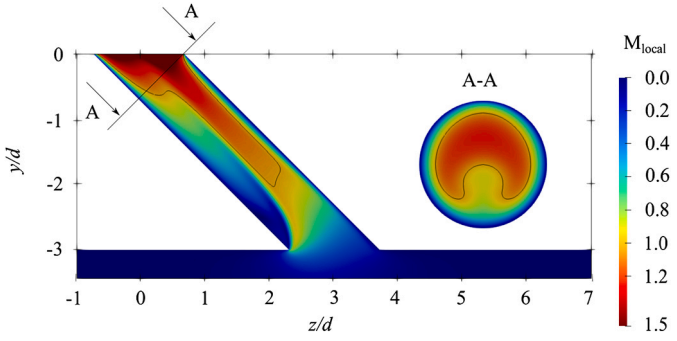

Fig. 3. Local Mach number distribution in a spanwise/wall-normal plane at $x = 0$ superimposed with contour line of $M_{local} = 1$ for case M7.2a. Crosssectional view of the flow in the injection pipe close to the pipe exit in the figure inset.

velocity components in both supersonic and hypersonic cases have a satisfactory agreement with the DNS data. Compared to the DNS data, there is a slight over-prediction of the near wall RMS of streamwise velocity component, which is common for LES. Partially some preliminary results were presented in the conference paper [38].

4.2. Jet-pipe flow

The jet in the hypersonic cases was injected at a smaller pressure than in the supersonic cases to avoid stronger jet expansion (due to the smaller pressure ratio p_∞/p_0 at $M_\infty = 7.2$), and to make the JIHCF cases (M7.2a, M7.2b and M7.2c) more comparable to the JISCF cases M2.5a and M2.5b (see Table 3). For the hypersonic cases, two plenum pressure values, $p^{pl} = 0.002p_0$ ($\equiv 10p_\infty$) and $0.003p_0$ ($\equiv 15p_\infty$), were considered, and for the JISCF cases M2.5a and M2.5b, the plenum pressure was $p^{pl} = p_0 \equiv 17p_\infty$ (see Table 3).

Due to the large pressure difference between plenum and crossflow, the flow in the injection pipe accelerates and attains sonic speed close to the plenum/pipe intersection. The 45° spanwise inclination of the injection pipe leads to an asymmetrical flow along the axial direction of the pipe. The mean flow inside the injection pipe, however, is symmetrical across the spanwise/wall-normal plane at $x = 0$. Also, shortly downstream of the plenum/pipe intersection, the flow separates locally and a small subsonic region forms. Hence, the flow is 3D in the injection pipe and supersonic ($M_{local} = 1.5 - 1.6$) close to the pipe exit on the flat-plate surface (see Fig. 3; similar observations were made for cases M7.2b, M7.2c, M2.5a and M2.5b and are therefore not shown here). From the cross-sectional view of the pipe flow close to the exit on the flat-plate surface, it is clear that the jet flow is underdeveloped with inflectional instability (see also [33]). Ramaswamy et al. [33] showed that injection-pipe lengths of about $10d$ are required to obtain a stable jet flow. Similar observations were also made for the flow in the jet-injection pipe in case M2.5b (see Fig. 4 in [14]), which indicates a negligible influence of M_∞, d, p^{pl} on the general topology of the flow in the injection pipe and the jet Mach number.

4.3. General flow topology and jet characteristics

The injected jet acts as an obstacle to the oncoming crossflow and induces an asymmetric and complex system of shock and vortical structures [14,39]. A bow shock is formed upstream of the injection location, and an envelop shock downstream of the injection location [40]. A visualization of the shock structures is shown for cases M7.2b, M7.2c and M2.5a in Fig. 4; the shock topology is similar for the other studied cases, hence, not shown here.

The angles of the bow and envelop shocks with respect to the streamwise direction are 11° and 8° for cases M7.2a and M7.2b, respectively. The angles are less steep than in the supersonic cases M2.5a and M2.5b, but a similar dependence on injection pressure (in the range $8 \le p^{pl}/p_\infty \le 17$) was observed for a JISCF case M2.5b [22]. For case M7.2c, the bow shock angle decreased to 9°, indicating a dependence on the injection-pipe diameter. The angle of the envelop shock remained constant. The angle of the bow and envelop shocks are 28° and 22° respectively for cases M2.5a and M2.5b, indicating no influence of the crossflow Reynolds number.

Injected jet expands in to the crossflow and forms a barrel shock terminating with a Mach disk for all cases. Reducing the injection pipe

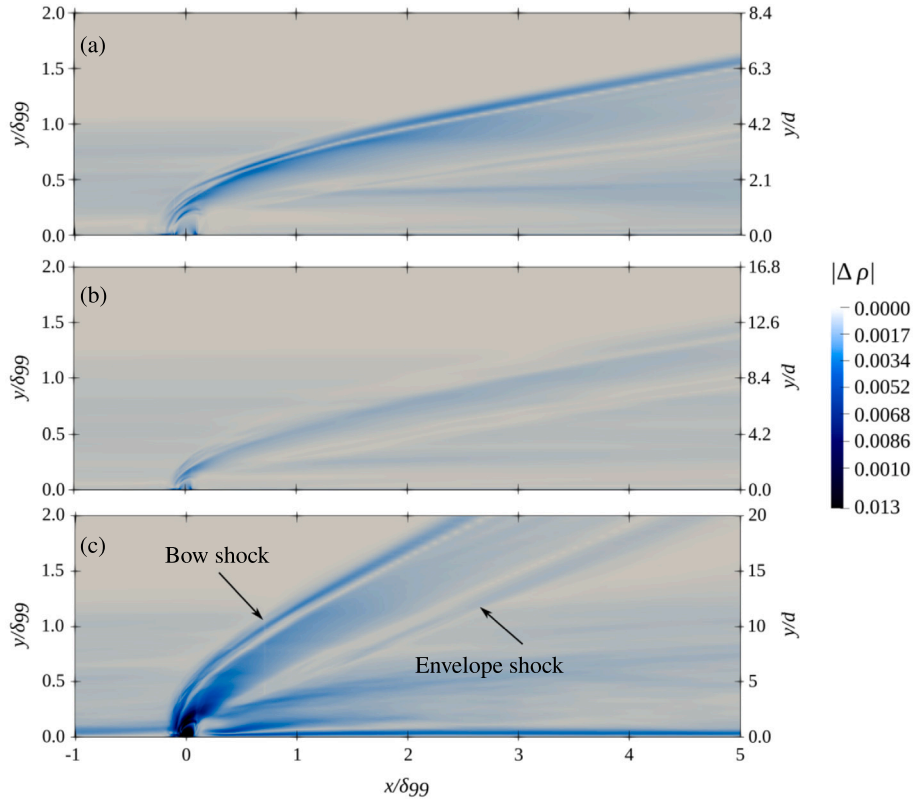

Fig. 4. Magnitude of the mean density gradient along the jet centerline ($z = 0$) in a streamwise/wallnormal plane for case (a) M7.2b, (b) M7.2c and (c) M2.5a.

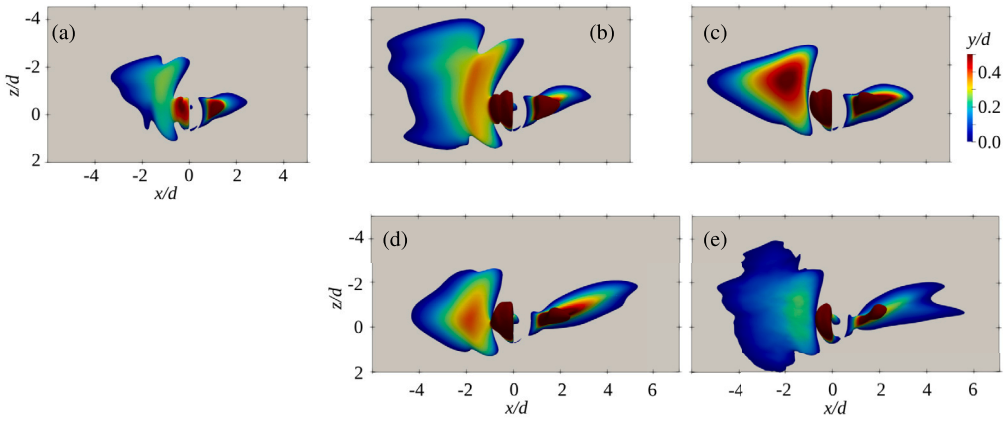

Fig. 5. Isosurface of $< u >= 0$ colored with y/d for case (a) M7.2a, (b) M7.2b, (c) M7.2c, (d) M2.5a, (e) M2.5b.

diameter results in a weaker jet injection with small C_μ (see Table 3). Therefore, the resulting shock structures are also weak in case M7.2c.

Injection of a jet into a crossflow induces separation regions both upstream and downstream of the jet (see Fig. 5, where the isosurface of $< u >= 0$ for all cases are shown). Due to the spanwise-inclined injection, the crossflow on the side of injection is largely diverged around the jet, and the crossflow on the opposite side interacts with the jet wake [14]. For spanwise-inclined injection, the induced separation regions are asymmetric. Their wall-normal extent increases with the injection pressure [22]. Similar observation is also made with hypersonic crossflow, see results of cases M7.2a and M7.2b shown in Fig. 5(a, b). Similarly, the size of the upstream recirculation decreases when the injection pipe diameter is reduced in case M7.2c while maintaining all conditions similar to M7.2b (see Figs. 5(b, c)). However, a significant effect of the crossflow Mach number on the upstream recirculation is not observed (see Figs. 5(c, d)).

However, in a low Reynolds number crossflow, the upstream separation region is smaller. Similar behavior was also observed for wall-normal jet injection [41]. At injection pressure $p^{\mathrm{pl}} = 17 p_\infty$, it extends up to $5d$ upstream for our supersonic case at $\mathrm{Re}_\tau \approx 1100$, whereas in the case M2.5a ($\mathrm{Re}_\tau = 245$), it extends up to $4d$ upstream. However, the recirculation region becomes narrower in the upstream direction resulting in a triangular shape (see Figs. 5(d, e)). This behavior is indeed an influence of Reynolds number (and not Mach number), since similar trends were also observed for wall-normal jet injection [41], moreover, similar topology of upstream separation region is observed for cases M7.2c and M2.5a (see Fig. 5(c, d)).

In the present JIHCF cases, the overall topology and its asymmetry are similar as for JISCF cases. However, the topology of the downstream separation region is similar for cases M7.2a, M7.2b, M7.2c and M2.5a: it is more streamlined to the crossflow, and it does not have the characteristic quasi-herringbone shape with two separation wings as ob-

served for JISCF by Sebastian et al. [14] (see case M2.5b in Fig. 5(e)). The formation of a herringbone-shaped downstream separation region is impeded by the low Re_τ of the crossflow, which leads to weaker interactions in the jet wake than for the M2.5b case. The secondary surface-trailing vortices are associated to the downstream separation region [14]. Therefore, the present result indicates different flow behavior close to the flat-plate surface in the injection near-field due to the low-Reynolds-number crossflow.

Jet properties were estimated by calculating the surface integral on a plane normal to the pipe axis, close to the pipe exit on the flat-plate surface. Due to the smaller injection pressure ($p^{pl}/p_\infty = 10$) in case M7.2a, the jet-to-free-stream pressure p^{jet}/p_∞, velocity V^{jet}/V_∞, density ρ^{jet}/ρ_∞, and momentum-flux ratio J, and momentum coefficient C_μ are consequentially smaller than in cases M2.5a and M2.5b. The jet-to-freestream pressure and velocity ratios are approximately 50% smaller; ρ^{jet}/ρ_∞ and J, however, are one and two orders of magnitude smaller than for the two JISCF cases, respectively, due to the smaller ρ^{pl}/ρ_∞.

In cases M7.2b and M7.2c, the injection pressure is increased to $p^{pl}/p_\infty = 15$, which results in a stronger jet (see Table 3). The jet-to-freestream pressure p^{jet}/p_∞ in cases M7.2b and M7.2c is closer to the reference case M2.5b, whereas other quantities are considerably smaller and in the same magnitude as in case M7.2a.

Earlier studies within the supersonic flow regime indicate Mach-number influences the jet characteristics: on the basis of schlieren visualizations of the wall-normal injection of Helium and Argon jets in crossflow at $M_\infty = 2$ and 3, Papamoschou and Hubbard [42] found that the momentum-flux ratio J is strongly dependent on jet Mach number M^{jet} for a fixed jet-exit pressure ratio ($p^{jet}/p_{\infty 2}$, where $p_{\infty 2}$ is the crossflow pressure after the bow shock), whereas the free-stream Mach number M_∞ only has a weak influence.

Our current results suggest that this behavior changes for hypersonic conditions, and that the influence of M_∞ on J increases at higher Mach number (see Table 3). For an equivalent p^{jet}/p_∞, momentum-flux-ratios J of the hypersonic cases M7.2b and M7.2c are one order of magnitude smaller than the supersonic cases M2.5a and M2.5b, however, the flow in the injection pipe and the jet Mach number M^{jet} is not influenced by M_∞ (see also Sec. 4.2). This observation also means that J is not an ideal injection parameter when comparisons of AJVG setups across different flow regimes with significantly varying Mach number are planned. When the injection pressure p^{pl} and the jet pressure p^{jet} are scaled with the corresponding freestream pressure p_∞, a quasi linear relation is observed between the injection and jet pressure (see Table 3). This indicates that the jet pressure close to the exit scales very well with the freestream pressure, making their ratio an ideal injection parameter in different Mach number regimes of the crossflow.

The jet-penetration behavior in the near field close to injection is directly related to the jet-induced separation regions [22]. The penetration depth of the jet into the crossflow was computed from the trajectory of the streamline passing through the jet center. The penetration curves shown in Fig. 6(a) and (b) are scaled with the corresponding δ_{99} and d, respectively.

In the far field $x/\delta_{99} \geq 10$, the penetration curves of cases M7.2a, M7.2b, and M7.2c diverge significantly due to their different δ_{99}/d ratios: for cases M7.2a and M7.2b, the jet penetrates up to $y = 0.8\delta_{99}$ (due to the smaller $\delta_{99}/d \approx 5$), indicating a stronger lift-off of the major counter-rotating vortex pair (CVP) into the boundary layer. On the other hand, when the jet diameter is reduced to $\tilde{d} = 0.5$ mm to match the δ_{99}/d of cases M2.5a and M2.5b (JIHCF case M7.2c), the near field jet penetration drops by a factor of four, indicating that the initial expansion of the jet in to the boundary layer strongly depends on the cross sectional area of the jet for a fixed crossflow and jet injection conditions.

In the far field, a similar penetration is observed for cases M7.2c, M2.5a and M2.5b due matching δ_{99}/d: compared to cases M7.2a and M7.2b, the major CVP in case M7.2c stays within $y = 0.5\delta_{99}$ due to larger $\delta_{99}/d \approx 10$.

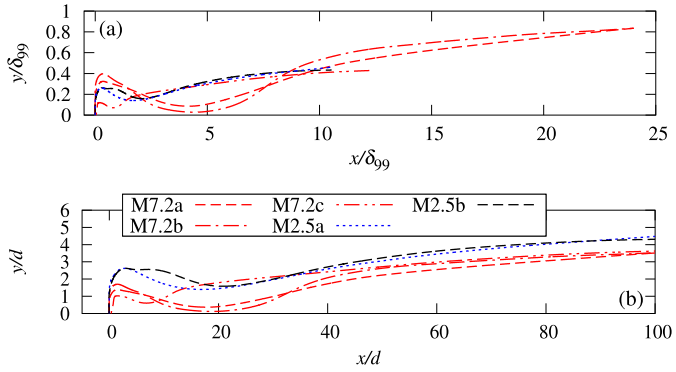

Fig. 6. Jet penetration scaled with (a) δ_{99}, and (b) d.

When scaled with d, the trends of all penetration curves are very similar: after an initial peak directly after injection, the penetration depth first decreases and then increases again, slowly approaching the respective maximum value. For case M7.2c, the approach of the maximum value after the local reduction happens much earlier than for all other cases ($x/d \approx 10$ instead of around $x/d = 20$). Both in the near field and far field regions, the penetration for the hypersonic cases is about 25% - 30% smaller than for cases M2.5a and M2.5b.

When the injection pressure is increased in case M7.2b, the penetration depth increases slightly, as previously observed for jets in supersonic crossflow (see [22]). However, although the p^{pl}/p_∞ values in cases M7.2b, M2.5a and M2.5b match, the penetration depth in the hypersonic case it is still lower than for JISCF cases due to smaller C_μ. Independent of Mach number M_∞, the jet-penetration depth thus can be amplified by increasing the injection pressure p^{pl}, and the near field jet expansion is dependent on the jet cross-sectional area. Moreover, the jet trajectory scales with d across different Mach number regimes.

Considering the adaptability of AJVGs at different flow regimes, these results thus indicate (a) p^{pl}/p_∞ as a more suitable control parameter, and (b) larger $\delta_{99}/d \approx 10$ to be more suitable for control purposes, because the jet stays within the boundary layer and thus induces less parasitic drag.

4.4. Coherent vortical structures

The interaction between jet and crossflow leads to the formation of vortical structures. In supersonic crossflow, the most prominent structure is the major CVP, which is also most relevant for separation-control purposes. An additional secondary counter-clockwise rotating (CCR) upper-trailing vortex and a surface-trailing CVP are also formed. The upper-trailing vortex merges with the major CVP to form an uneven CVP [14]. The major CVP transfers momentum from the outer region of the boundary layer to the near-wall region, resulting in a fuller velocity profile that eventually makes the boundary layer more resistant to separation.

Injection of the jet significantly modifies the mean flow. Therefore, the Q-criterion technique was applied to the mean flow to identify the coherent vortical structures in the flow field. Results of the Q-criterion for JIHCF cases M7.2a and M7.2b are shown in Figs. 7(a) and (b), respectively. The major CVP is clearly visible, with a stronger clockwise rotating (CR) major vortex that persists up to about $25d$ downstream of the injection location. The size and downstream extent of the major CVP increase with injection pressure; similar behavior has been observed for JISCF (see [22]). Also horseshoe vortices that originate from the upstream separation region are visible. In comparison with the supersonic JISCF cases, these horseshoe vortices do not breakdown immediately downstream of injection and have a longer lifespan: they persist up to $x = 5d - 8d$. You et al. [43] studied wall-normal jet injection with $J = 0.35$ in a crossflow at $M_\infty = 2.4$, and also observed horseshoe vortex upto 5d downstream of the jet injection location. The horseshoe vortex

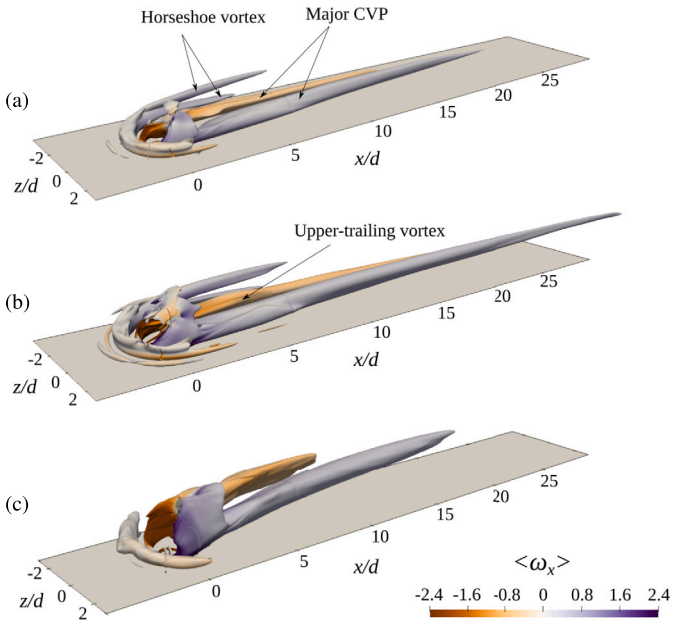

Fig. 7. Isosurface of Q-criterion ($Q = 0.07$) colored with $< \omega_x >$ for cases (a) M7.2a, (b) M7.2b and (c) M2.5a.

originates upstream of the injection location, then gradually turns and streamlines with the crossflow. Q-criterion of the case M2.5a is shown in Fig. 7(c). In both JISCF cases, the horseshoe vortices exist only in the immediate vicinity due to larger J compared to the JIHCF cases (see Table 3) and resulting in a better mixing.

Recently, we showed that the formation of an upper-trailing vortex pair in supersonic crossflow depends on jet-injection pressure, and there exists a strong interplay between the jet-spacing and injection pressure that has the major influence on the control-effectiveness of the air-jet vortex-generators. [22]. We showed that the upper-trailing vortex forms in supersonic crossflow when the jet pressure (p^{jet}) is approximately one order larger than the freestream pressure. High injection pressures or momentum-flux ratios can cause highly under-expanded jets, which consequently enhance the Mach-disk dynamics, resulting in the formation of an upper-trailing CVP [22]. At low injection pressures, the upper-trailing vortex disappears and a symmetric CVP forms even for spanwise-inclined jet injection. However, all cases in the above mentioned study considered jets with $J > 1$ (see Ref. [22] for details).

In the current JIHCF, a CCR upper-trailing vortex forms when the injection pressure is increased to $p^{\text{pl}}/p_\infty = 15$ in case M7.2b, but not for $p^{\text{pl}}/p_\infty = 10$ (case M7.2a; see Figs. 7(a, b)). This injection-pressure dependence thus seems to occur across a wide range of Mach numbers. The upper-trailing vortex is less prominent in the hypersonic than in the supersonic case, though, due to the slightly weaker jet-injection conditions. Furthermore, the low Reynolds number of the crossflow in cases M7.2a, M7.2b, M7.2c and M2.5a results in weaker near-wall dynamics in the jet wake, thus preventing the formation of surface-trailing CVPs as observed for case M2.5b with higher Reynolds number (see also Fig. 5 and Ref. [14]).

To further quantify the influence of injection and flow conditions (δ_{99}/d, p^{pl}/p_∞, M_∞ and Re_τ) on the vortical structures, we consider the spanwise/wall-normal distribution of the streamwise component of the mean vorticity shown in Fig. 8. To access the influence of jet injection on the boundary layer, the vorticity is normalized with δ_{99}. However, the results and trends are very similar when u_∞ or a_0 are used to normalize the vorticity.

In the near-field region ($x = 5d$) of JIHCF case M7.2a, a symmetric major CVP with a width of approximately $5d$ indicates the absence of a secondary upper-trailing vortex. A symmetric CVP was also observed for low-pressure injection in supersonic crossflow [22]. Also, a significantly larger horseshoe vortex is observed in the direction of injection ($-z$-side). However, the horseshoe vortex does not have a significant effect on the downstream boundary layer flow.

Upon an increase in injection pressure, the major CVP strengthens and increases its size to approximately $6d$, and looses it symmetry due to the formation of the secondary CCR upper-trailing vortex (see also Fig. 7(b)). The upper-trailing vortex is not as prominent as it is in the JISCF case, therefore, the axis of both major vortices lies at the same wallnormal distance from the flatplate surface, whereas, for cases M2.5a and M2.5b the CCR major vortex lies above the CR major vortex at $x = 5d$ (see Figs. 8(j, m)). However, size and asymmetry of the vortical structures depend on the injection pressure to a similar extent as for JISCF [22].

A reduction of the injection-pipe diameter (case M7.2c) does not change the characteristics of the major CVP (compare with case M7.2b). The spanwise extent of the horseshoe vortex, however, decreases, which indicates that the lateral divergence of the crossflow on the $-z$-side reduces significantly with the smaller injection-pipe diameter. Moreover, the low J in the hypersonic cases prevent the breakdown of the horseshoe vortex, allowing it to persist until $x = 5d - 8d$ downstream (see also Fig. 7).

JISCF cases M2.5a and M2.5b generate comparatively larger major CVP than the JIHCF cases due to larger J.

For equivalent injection pressure p^{pl}/p_∞, the size of the CVP structure scales with the injection-pipe diameter, and it is independent of the boundary-layer thickness δ_{99} (see Figs. 8(d, g, j, m)).

Farther downstream, at location $x = 10d$, the strength of the vorticity has dropped significantly, and the major CVP has slightly lifted off of the flat-plate surface. The topology of the major CVP, however, is maintained from $x = 5d$ in this hypersonic crossflow. In supersonic case M2.5b, the CCR major vortex is now kidney-shaped and the CR major vortex is circular. The major CVP has rotated around its axis, and both vortices are now at about the same distance from the wall. However, in the case M2.5a, the CCR vortex has not fully evolved into a kidney-shaped structure. Therefore, from the vorticity distribution of cases M2.5a and M2.5b, it can be inferred that major CVP in the low Reynolds number crossflow (case M2.5a) mix slightly less efficiently than in the high Reynolds number crossflow (case M2.5b). This observation agrees with the studies of Wang et al. [41] with wall-normal jet injection. Wang et al. [41] studied the flow fields of perpendicular jets in supersonic crossflow at $\text{M}_\infty = 1.6$. They reported that interactions between the large upstream separation region and the shear layer in the jet plume at higher Reynolds numbers initiate the turbulent breakdown of the jet plume and induce the formation of instantaneous large vortical features. For a lower Reynolds number, the upstream separation region is small and stable, and the upstream jet expansion is weaker; the subsequent jet mixing with the crossflow is therefore less efficient [41].

At $x = 20d$, the vorticity of JIHCF cases M7.2a, M7.2b and M7.2c has dropped further. The size of the major CVP is still unchanged compared to the injection-near field. In the supersonic cases M2.5a and M2.5b, the major CVP has enlarged in the corresponding downstream evolution due to mixing with the crossflow. This difference in behavior indicates that the major CVP in the hypersonic crossflow is more localized and the momentum introduced by the jet injection is less efficiently redistributed in the boundary layer due to the low J in the JIHCF cases. These results agree with the findings of You et al. [43] for wall-normal jets, where they reported jets with low J result in weak mixing with crossflow by studying injection of a jet with $J = 0.35$ in a supersonic crossflow at $\text{M}_\infty = 2.4$. However, such a behavior would be beneficial when jets are used for cooling applications.

Reducing the injection-pipe diameter (case M7.2c) leads to a weaker CVP in the far field (compare with case M7.2b in Figs. 8(f) and (i)). The cross sectional area of the jet-injection pipe in case M7.2c is four times smaller than for case M7.2b, which results in lower momentum influx (see also Table 3).

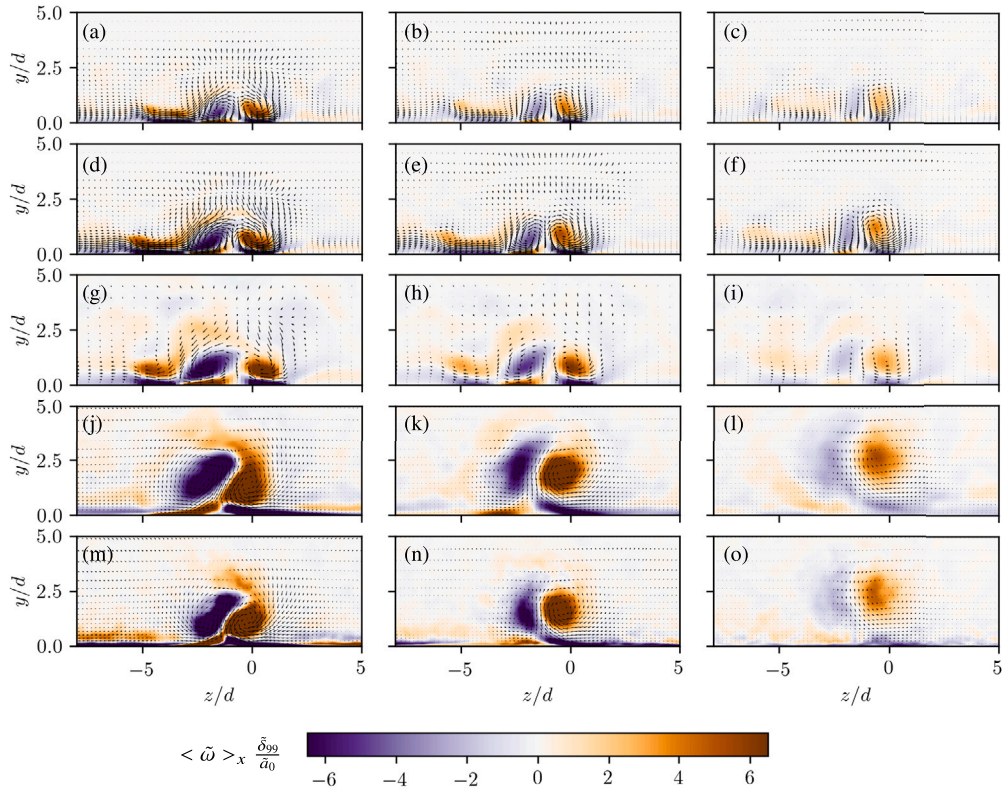

Fig. 8. Distribution of $< \omega_x >$ in a spanwise/wall-normal plane at (a, d, g, j, m) $x = 5d$; (b, e, h, k, n) $x = 10d$; and (c, f, i, l, o) $x = 20d$ for case (a-c) M7.2a; (d-f) M7.2b; (g-i) M7.2c, (j-l) M2.5a and (m-o) M2.5b.

In summary, the injection pressure ratio p^{pl}/p_∞ is a suitable control parameter to characterize the jet penetration (see Fig. 6(b)) and overall topology of vortical structures (see Fig. 8) across both supersonic and hypersonic M_∞. However, the momentum redistribution effected by the jet and the mixing with the boundary layer is strongly dependent on J and/or C_μ of the injection setup and weakly dependent on the Re_τ of the crossflow into which the jet is injected.

4.5. Boundary layer statistics

We now discuss the effect of jet injection on the boundary-layer statistics. A comparison of the downstream evolution of the mean and RMS of the streamwise velocity component along $z = 0$ for cases M7.2a, M7.2b, M7.2c, M2.5a and M2.5b is shown in Fig. 9(a). The mean velocity and wall-normal distance are scaled with the corresponding u_∞ and δ_{99}, respectively. The results are also compared with the corresponding uncontrolled boundary-layer data of the respective cases (red solid line: uncontrolled C1 boundary layer, blue solid line: uncontrolled C2 boundary layer and black solid line: uncontrolled C3 boundary layer).

For all controlled cases, the near-field ($x = 5d$) mean-velocity profile features multiple inflection points due to the jet injection. Compared to the supersonic case M2.5b, the velocity deficit is stronger for the JIHCF cases and M2.5a, with local minima of about $0.2u_\infty$ and $0.4u_\infty$, respectively at $y \approx 0.2\delta_{99}$. The larger wake region in cases M7.2a, M7.2b, and M2.5a is associated with the major CVP, and it is visible between $0.1 \leq y/\delta_{99} \leq 0.4$. Moreover, a local increase in the velocity at $y \approx 0.3\delta_{99}$ is also not observed for the JIHCF cases (M7.2a, M7.2b, and M7.2c) and JISCF case M2.5a.

When the injection pressure is increased, the inflectional points are displaced further away from the wall (see mean velocity profiles of cases M7.2a and M7.2b at $x = 5d$). Similar behavior is also observed for JISCF [22].

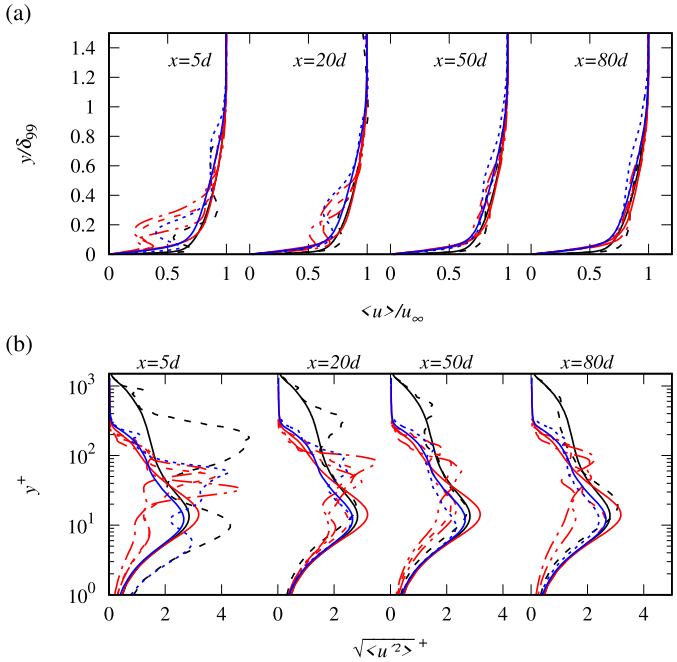

Fig. 9. Downstream evolution of (a) mean and (b) RMS of streamwise velocity along $z = 0$ at locations $x/d = 5, 20, 50$, and 80. Solid and dashed lines are used for the uncontrolled and controlled cases, respectively. Red, blue and black colored lines are used for jet-injection in crossflows C1, C2 and C3, respectively. For legends see Fig. 6.

When the injection-pipe diameter is reduced, the location of the inflectional point moves proportionally closer to the wall, from $y = 0.2\delta_{99}$ to $y = 0.1\delta_{99}$ for cases M7.2b and M7.2c, respectively.

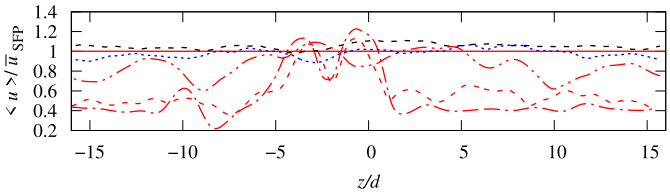

Fig. 10. Spanwise distribution of $< u >$ at $y = 0.1\delta_{99}$. For legends see Fig. 6.

Farther downstream, at $x = 20d$, the immediate influence of jet injection has decreased and the boundary layer is undisturbed for $y \geq 0.6\delta_{99}$. A fuller region near the wall begins to appear for both the JISCF and JIHCF cases. Due to the stronger vortex lift off in cases M7.2a and M7.2b (smaller $\delta_{99}/d \approx 5$), the fuller regions are displaced farther away from the wall (see profiles at $x = 50d$ and $80d$).

The major CVP is weaker in case M7.2c due to the smaller injection-pipe diameter. The fuller region near the wall is therefore less pronounced, and thus the separation-control effectiveness reduces.

Increasing the momentum influx with the smaller injection pipe to compensate this decrease is not a suitable approach, though: a stronger bow shock would be caused upstream of the injection location, which would result in stronger lift off of the major CVP, and thus the fuller region would be displaced even farther from the wall.

Szwaba et al. [10] experimentally studied the influence of jet diameter in a row array of AJVGs, installed to control a SWBLI in a Mach 1.43 flow. They found that AJVG arrays with $\delta_{99}/d \geq 4$ are more suitable to control SWBLI, and that an increase in jet diameter results in increased flow unsteadiness and pressure load due to the SWBLI. More recently, spacings of $7d - 11d$ between the jets with $\delta_{99}/d \approx 10$ were identified as most suitable [23]. This spacing allows for jet/jet interactions that cause stronger downwash. As a consequence, the transfer of momentum to the near-wall region is enhanced, which makes the flow more resistant to separation. A detailed description of the jet/jet interactions with spanwise-inclined injection is given in Sebastian and Schreyer [23].

A comparison of the RMS of the streamwise velocity component for all cases is shown in Fig. 9(b). For the supersonic cases M2.5a and M2.5b, two peaks are observed in the profile closely downstream of injection ($x \leq 5d$): a buffer-layer peak due to wall turbulence and an outer-layer peak due to the injection. In the present hypersonic cases, however, only a single peak is visible ($y^+ \approx 30 - 80$). Cases M7.2a, M7.2b, M7.2c and M2.5a have comparable $\mathrm{Re}_\tau \approx 215 - 245$. Even though the displacement between the inner- and outer-layer regions of the boundary layer is very small two peaks in the RMS profile is evident in case M2.5a. This indicates that the observed effect in the JIHCF cases is due to the lower J of the injection. Farther downstream, the peak in the RMS profile for the JIHCF cases drops gradually.

For JISCF cases M2.5a and M2.5b, the near-wall turbulence has recovered around $x = 20d$. For JIHCF case M7.2a, this recovery process is completed only at $x = 80d$, and for high-injection-pressure cases M7.2b and M7.2c the near-wall turbulence has not recovered within $100d$. This observed difference to the JISCF case M2.5 is related to the low J of the jet injection in the hypersonic crossflow: the major CVP generated in the JIHCF cases acts more localized and mixes less efficiently with the crossflow. Hence, the major CVP still influences the mean flow at larger distances downstream of injection and thus slows down the recovery of the near-wall turbulence.

To further investigate the spanwise influence of the major CVP on the crossflow, we analyze the spanwise mean-velocity distribution at the location where fuller boundary-layer profiles were observed in Fig. 10 ($y \approx 0.1\delta_{99}$). The velocity distribution is normalized with the corresponding mean value of the undisturbed case, such that $\langle u \rangle / \langle u \rangle_{\mathrm{SFP}} > 1$ indicates regions in the boundary layer where profiles are fuller than in the uncontrolled case. In the supersonic M2.5b case, near-wall fullness is observed in the entire spanwise domain ($-16 \leq z/d \leq 16$), with approximately 10% and 5% higher velocity compared to the undisturbed case on the $+z$ and $-z$ sides, respectively. For all hypersonic cases, however, the profiles are only fuller at the location of the major CVP ($-5 \leq z/d \leq 2$), which indicates a strong influence of both major vortices. As in the JISCF case, the near-wall velocity of the JIHCF cases on the $+z$-side is stronger compared to the $-z$-side since the CR major vortex is stronger. Case M2.5a has similar velocity distribution as case M2.5b, however, due to the low Reynolds number of the crossflow the mixing efficiency is slightly weaker compared to case M2.5b (see Fig. 10).

Due to the larger $\delta_{99}/d \approx 10$, the velocity deficit for case M7.2c is smaller than for cases M7.2a and M7.2b. An increase in jet injection-pipe diameter results in stronger jet penetration (see Fig. 6(a)) and lift off of the CVP in to the boundary layer. The fuller region is thus displaced farther away from the wall and the deficit in the near wall region increases (see velocity distribution for case M7.2b in Fig. 10).

The present results indicate the boundary-layer-to-pipe-diameter ratio (δ_{99}/d) as a critical parameter in determining how the jet injection influences the boundary-layer flow. Combining Figs. 6(a) and 9, it can be inferred that the lift-off of the major CVP can be delayed by considering larger δ_{99}/d. Since delayed lift-off results in a prolonged transfer of momentum to the near-wall region, an increase of δ_{99}/d would also make the boundary layer less susceptible to separation. However, reduced momentum injection with smaller d is an imminent issue, which results in a weaker CVP in the far field. Increasing the injection pressure is one solution to increase the momentum influx, however, this can counter the control efficiency by causing stronger blockage to the oncoming flow. Viable solutions are to (a) either inject a row of jets with spacing $7d - 11d$ to allow jet/jet interactions that increase the downwash [23], or (b) consider different fluid properties for the jet and the crossflow.

5. Conclusions

Motivated by the need to develop effective methods to control shock-induced separation for aerospace-engineering applications, we strive for a better understanding of the flow physics relevant to air-jet vortex generators. Separation-control studies in hypersonic flows are particularly scarce. Since the injection of spanwise-inclined air-jets (via AJVGs) is an efficient means to control shock-induced flow separation in supersonic and transonic flows, the primary objective of this work was to broaden the knowledge, understanding, and applicability of AJVGs into the hypersonic flow regime. Therefore, numerical simulations of the injection of a single spanwise-inclined jet in supersonic and hypersonic crossflows at $\mathrm{M}_\infty = 7.2$; $\mathrm{Re}_\theta = 3500$ and $\mathrm{M}_\infty = 2.5$; $\mathrm{Re}_\theta = 1570$ were performed to a) study JICF in the hypersonic flow regime that is relevant for novel space-transportation systems, b) analyze the effect of crossflow Mach number on the jet/crossflow interaction, and c) identify the jet-injection parameter that is most suitable and meaningful across a wide range of flow conditions.

To achieve these objectives, we carried out a systematic parameter study. We studied the influence of (1) injection-pressure-to-freestream-pressure ratio (p^{pl}/p_∞), (2) boundary-layer-to-jet-diameter ratio (δ_{99}/d), (3) Mach number M_∞, and (4) friction Reynolds number Re_τ of the crossflow boundary layer on the jet/crossflow interactions. Results were compared with our previous study of an equivalent injection setup in supersonic crossflow at $\mathrm{M}_\infty = 2.5$ and $\mathrm{Re}_\theta = 7000$. The general characteristics of the jet/crossflow interactions are similar in the supersonic and hypersonic regimes.

The present results indicate that the crossflow Mach number has a negligible influence on the flow structure in the injection pipe and on the jet Mach number. The characteristics of the jet are mainly determined by the injection pressure. On the other hand, the results reveal that the influence of M_∞ on the momentum-flux ratio J increases at higher Mach numbers, indicating that (the commonly used parameter) J is not an ideal control parameter when comparisons of AJVG setups across different flow regimes are considered. Instead, we identified the

injection pressure p^{pl}/p_∞ as a suitable control parameter to characterize and compare jet/crossflow interactions in supersonic and hypersonic crossflows (including the induced vortical structures and their downstream evolution).

Injection of a spanwise-inclined jet results in an asymmetric flow topology both in supersonic and hypersonic crossflow, with a complex system of shock and vortical structures. The size of the major CVP scales with the injection-pipe diameter and tends to increase with the injection pressure in both JISCF and JIHCF cases; it is independent of the boundary-layer thickness. However, the injection of a jet with low J in the hypersonic crossflow affects both the major counter-rotating vortex pair and some secondary vortices: the momentum redistribution in the boundary layer is less efficient and the horseshoe vortex is larger compared to the jet injection case with larger J. These observations agree with the findings for wall-normal jet injection with low J in supersonic crossflow.

Low Re_τ of the crossflow results in slightly weaker interactions in the jet wake: surface-trailing vortices are missing and mixing is weaker. Similar behavior has been observed for perpendicular jet injection in supersonic crossflow. Also, at low Re_τ, the jet-induced upstream separation region is smaller, and the formation of a herringbone-shaped downstream separation is impeded both in the supersonic and hypersonic regimes. However, the mixing efficiency is only slightly effected by Re_τ in comparison to J.

The downstream developments of jet penetration into the respective boundary layers show similar trends in supersonic and hypersonic flow when scaled with the injection-pipe diameter. The jet penetration is strongly dependent on δ_{99}/d. At smaller values of δ_{99}/d, stronger jet penetration into the boundary layer amplifies the lift-off of the CVP. Consequently, the fuller region in the boundary layer (achieved due to the increased mixing effected by the major CVP) shifts away from the wall. For separation-control purposes, a larger δ_{99}/d is therefore advisable.

One imminent issue with larger δ_{99}/d or smaller d is a reduction of the momentum influx, which eventually results in the formation of weaker major CVP. This can be effectively countered either by injecting a row of jets at moderate spacing of $7d - 11d$, or by changing the fluid properties of the jet.

For both spanwise-inclined JISCF and JIHCF cases, the velocity near the wall is stronger on the $+z$-side (opposite to the direction into which the jet is injected) compared to the $-z$-side due to the stronger CR major vortex. However, due to the low J in the hypersonic cases, the jet is not efficiently mixed and redistributed in the boundary layer. This behavior is characteristic for low J jet injection; it is independent of the Mach number, as similar observations have also been reported for low J jet injection in supersonic crossflow. As a result, the major CVP is preserved for a larger downstream distance, thus strongly affecting the near-wall flow and delaying the regeneration of wall turbulence. Owing to this persistence of the major CVP, jets with low J could be beneficial for use in cooling applications. However, further studies are needed to evaluate the capabilities of low J jet injection.

Our previous study [14] has shown that while the jet orientation affects the flow topology, the general characteristics of jet/crossflow interactions are unchanged for a single jet. However, these topology modifications most probably affect interactions between adjacent jet-induced structures, and such jet/jet interactions crucially affect the separation-control effectiveness when multiple jets are arranged in an array configuration [23]. Therefore, different jet orientations in array configurations in a wide range of flow regimes and conditions shall be studied in the future to advance the application of AJVGs for both separation control and cooling purposes.

CRediT authorship contribution statement

Robin Sebastian: Formal analysis, Investigation, Methodology, Software, Validation, Visualization, Writing – original draft, Writing – review & editing, Conceptualization. **Anne-Marie Schreyer:** Conceptualization, Funding acquisition, Writing – review & editing.

Declaration of competing interest

The authors declare that they have no known competing financial interests or personal relationships that could have appeared to influence the work reported in this paper.

Data availability

Data will be made available on request.

Acknowledgements

This work was supported by the Deutsche Forschungsgemeinschaft (German Research Foundation) within the framework of the Emmy Noether Programme (grant / project number 326485414). We would also like to thank the High-Performance Computing Center, Stuttgart (HLRS) for providing the computational resources within a large-scale project of the Gauss Center for Supercomputing (GCS). Finally, we would like to thank Lukas Karl Pluta for preparing the computational grid used in testcase M7.2c.

References

[1] W. Wong, The application of boundary layer suction to suppress strong shock-induced separation in supersonic inlets, in: 10th AIAA Propulsion Conference, 1974.
[2] H. Pearcey, Introduction to shock-induced separation and its prevention by design and boundary layer control, in: G. Lachmann (Ed.), Boundary Layer and Flow Control, Pergamon, 1961, pp. 1166–1344.
[3] R.A. Wallis, The use of air jets for boundary layer control, Tech. rep., Aerodynamic Notes, vol. 110, Aerodynamic Research Lab, Australia, 1952.
[4] L. Yue, X. Xu, X. Chang, Theoretical analysis of effects of boundary layer bleed on scramjet thrust, Sci. China, Phys. Mech. Astron. 56 (10) (2013) 1952–1961, https://doi.org/10.1007/s11433-013-5257-46.
[5] J.C. Lin, Review of research on low-profile vortex generators to control boundary-layer separation, Prog. Aerosp. Sci. 38 (4) (2002) 389–420, https://doi.org/10.1016/S0376-0421(02)00010-6.
[6] P.L. Blinde, R.A. Humble, B.W. van Oudheusden, F. Scarano, Effects of micro-ramps on a shock wave/turbulent boundary layer interaction, Shock Waves 19 (2009) 507–520, https://doi.org/10.1007/s00193-009-0231-9.
[7] Y. Kamotani, I. Greber, Experiments on a turbulent jet in a cross flow, AIAA J. 10 (11) (1972) 1425–1429, https://doi.org/10.2514/3.50386.
[8] R. Szwaba, P. Flaszyński, J.A. Szumski, P. Doerffer, Influence of air cooling and air-jet vortex generator on flow structure in turbine passage, TASK Quarterly: Sci. Bull. Acad. Computer Centre in Gdansk 19 (2) (2015) 153–166.
[9] R. Szwaba, Comparison of the influence of different air-jet vortex generators on the separation region, Aerosp. Sci. Technol. 15 (1) (2011) 45–52, https://doi.org/10.1016/j.ast.2010.06.001.
[10] R. Szwaba, Influence of air-jet vortex generator diameter on separation region, J. Therm. Sci. 22 (4) (2013) 294–303, https://doi.org/10.1007/s11630-013-0627-9.
[11] S.B. Verma, C. Manisankar, Control of compression-ramp-induced interaction with steady microjets, AIAA J. 57 (7) (2019) 2892–2904, https://doi.org/10.2514/1.J057509.
[12] M.Y. Ali, F. Alvi, Jet arrays in supersonic crossflow — an experimental study, Phys. Fluids 27 (12) (2015) 126102, https://doi.org/10.1063/1.4937349.
[13] R.A. Wallis, On the control of shock-induced boundary-layer separation with discrete air jets, Tech. rep., Aeronautical Research Council CP 595, 1958.
[14] R. Sebastian, T. Lürkens, A.-M. Schreyer, Flow field around a spanwise-inclined jet in supersonic crossflow, Aerosp. Sci. Technol. 106 (2020) 106209, https://doi.org/10.1016/j.ast.2020.106209.
[15] D.P. Ramaswamy, A.-M. Schreyer, Control of shock-induced separation of a turbulent boundary layer using air-jet vortex generators, AIAA J. 59 (3) (2021) 927–939, https://doi.org/10.2514/1.J059674.
[16] A.-M. Schreyer, D. Sahoo, O.J.H. Williams, A.J. Smits, Influence of a microramp array on a hypersonic shock-wave/turbulent boundary-layer interaction, AIAA J. 59 (6) (2021) 1924–1939, https://doi.org/10.2514/1.J059925.
[17] D.P. Ramaswamy, A. Barklage, A.-M. Schreyer, Separation control using air-jet vortex generators in a hypersonic shock-induced boundary-layer separation, Deutsche Gesellschaft, für Luft- und Raumfahrt - Lilienthal-Oberth e.V, https://doi.org/10.25967/530277.
[18] A.-M. Schreyer, D. Sahoo, O.J.H. Williams, A.J. Smits, Experimental investigation of two hypersonic shock/turbulent boundary-layer interactions, AIAA J. 56 (12) (2018) 4830–4844, https://doi.org/10.2514/1.J057342.

[19] S.E. Guarini, R.D. Moser, K. Shariff, A. Wray, Direct numerical simulation of a supersonic turbulent boundary layer at Mach 2.5, J. Fluid Mech. 414 (2000) 1–33, https://doi.org/10.1017/S0022112000008466.
[20] S. Priebe, P. Martin, Direct numerical simulation of a hypersonic turbulent boundary layer on a large domain, in: 41st AIAA Fluid Dynamics Conference and Exhibit, 2011.
[21] R. Sebastian, A.-M. Schreyer, Flow fields around spanwise-inclined elliptical jets in supersonic crossflow, Eur. J. Mech. B, Fluids 94 (2022) 299–313, https://doi.org/10.1016/j.euromechflu.2022.03.008.
[22] R. Sebastian, D.P. Ramaswamy, A.-M. Schreyer, Spanwise-inclined jets in supersonic crossflow: effects of injection-pressure and separation-control effectiveness, AIAA J. 61 (9) (2023) 3833–3847, https://doi.org/10.2514/1.J062286.
[23] R. Sebastian, A.-M. Schreyer, Influence of jet spacing in spanwise-inclined jet injection in supersonic crossflow, J. Fluid Mech. 946 (2022), https://doi.org/10.1017/jfm.2022.597.
[24] A. Lintermann, M. Meinke, W. Schröder, Zonal Flow Solver (ZFS): a highly efficient multi-physics simulation framework, Int. J. Comut. Fluid Dyn. 34 (7–8) (2020) 458–485, https://doi.org/10.1080/10618562.2020.1742328.
[25] J. Boris, F. Grinstein, E. Oran, R. Kolbe, New insights into large eddy simulation, Fluid Dyn. Res. 10 (4–6) (1992) 199–228, https://doi.org/10.1016/0169-5983(92)90023-P.
[26] M.-S. Liou, C.J. Steffen, A new flux splitting scheme, J. Comput. Phys. 107 (1) (1993) 23–39, https://doi.org/10.1006/jcph.1993.1122.
[27] M. Meinke, W. Schröder, E. Krause, T. Rister, A comparison of second- and sixth-order methods for large-eddy simulations, Comput. Fluids 31 (4–7) (2002) 695–718, https://doi.org/10.1016/S0045-7930(01)00073-1.
[28] V. Venkatakrishnan, Convergence to steady state solutions of the Euler equations on unstructured grids with limiters, J. Comput. Phys. 118 (1) (1995) 120–130, https://doi.org/10.1006/jcph.1995.1084.
[29] W. El-Askary, W. Schroeder, M. Meinke, Les of compressible wall-bounded flows, in: 16th AIAA Computational Fluid Dynamics Conference, 2003.
[30] B. Roidl, M. Meinke, W. Schröder, Numerical investigation of shock wave boundary-layer interaction using a zonal rans-les ansatz, in: W.E. Nagel, D.B. Kröner, M.M. Resch (Eds.), High Performance Computing in Science and Engineering '10, Springer, Berlin, Heidelberg, 2011, pp. 369–383.
[31] R. Sebastian, A.-M. Schreyer, Control of SWBLI in a 24deg compression ramp flow with air-jet vortex-generator, in: AIAA SCITECH 2023 Forum, American Institute of Aeronautics and Astronautics, 2023.
[32] R. Sebastian, A.-M. Schreyer, Forced injection of a spanwise-inclined jet in supersonic crossflow, AIAA J. 62 (1) (2024) 52–64, https://doi.org/10.2514/1.J063323.
[33] D.P. Ramaswamy, R. Sebastian, A.-M. Schreyer, Effects of jet-injection-pipe length on the flow-control effectiveness of spanwise-inclined jets in supersonic crossflow, Phys. Rev. Fluids 8 (11) (2023), https://doi.org/10.1103/PhysRevFluids.8.113902.
[34] R. Sebastian, A.-M. Schreyer, Forced control of SWBLI in a 24deg compression ramp flow with air-jet vortex-generator, in: AIAA AVIATION 2023 Forum, American Institute of Aeronautics and Astronautics, 2023.
[35] L. Duan, I. Beekman, M.P. Martín, Direct numerical simulation of hypersonic turbulent boundary layers. Part 2. Effect of wall temperature, J. Fluid Mech. 655 (2010) 419–445, https://doi.org/10.1017/S0022112010000959.
[36] B. Roidl, A zonal method to efficiently simulate viscous flows, Ph.D. thesis, RWTH Aachen University, 2012.
[37] A. Trettel, J. Larsson, Mean velocity scaling for compressible wall turbulence with heat transfer, Phys. Fluids 28 (2) (2016) 026102, https://doi.org/10.1063/1.4942022.
[38] R. Sebastian, A.-M. Schreyer, Influence of crossflow Mach number on spanwise-inclined jet injection, in: AIAA SCITECH 2022 Forum, American Institute of Aeronautics and Astronautics, 2022.
[39] Z.A. Rana, B. Thornber, D. Drikakis, Transverse jet injection into a supersonic turbulent cross-flow, Phys. Fluids 23 (4) (2011) 046103, https://doi.org/10.1063/1.3570692.
[40] M. Morkovin, C. Pierce, C.E. Craven, Interaction of a side jet with a supersonic main stream, Tech. rep., Bull., vol. 35, Engg. Res. Inst, Univ. Michigan, 1952.
[41] Z. Wang, H. Wang, M. Sun, N. Qin, Hybrid Reynolds-averaged Navier-Stokes/large-eddy simulation of jet mixing in a supersonic crossflow, Sci. China, Technol. Sci. 56 (2013) 1435–1448, https://doi.org/10.1007/s11431-013-5189-2.
[42] D. Papamoschou, D. Hubbard, Visual observations of supersonic transverse jets, Exp. Fluids 14 (1993) 468–476, https://doi.org/10.1007/BF00190201.
[43] Y. You, H. Lüdeke, K. Hannemann, On the flow physics of a low momentum flux ratio jet in a supersonic turbulent crossflow, Europhys. Lett. 97 (2) (2012) 24001, https://doi.org/10.1209/0295-5075/97/24001.